Signal Space Decoupled Stream Splitting for Low Latency Downlink MIMO WBANs

Gunjit Arora, Satya Kumar Vankayala, and Manoj Thomas
Network Call & OAM Team, Samsung R&D Institute, Bengaluru, India, 560037
Email: gunjit_a@ece.iitr.ac.in, satyakumar.v@samsung.com, manoj.thomas@samsung.com

***Abstract*—Wireless body area networks (WBANs) require ultra-low decoding latency and reliable control-signal detection at on-body actuators to promptly respond to abnormal patient conditions. These requirements are challenged by strong intra- and inter-WBAN interference, as well as by the computational overhead of successive interference cancellation (SIC) in conventional rate-splitting multiple access (RSMA) based WBANs. To address these issues, we propose a signal-space decoupled stream-splitting multiple access (SDSMA) scheme for downlink multiple-input multiple-output (MIMO) WBANs, in which each transmitted control signal consists of an orthogonally mapped composite common stream (CCS) and multiple private streams (PSs) across signal-space dimensions. This design enables interference-free CCS detection and parallel CCS/PS decoding without SIC, thereby reducing receiver complexity and decoding latency. From a signal-processing perspective, we perform a constellation-based error analysis of SDSMA for arbitrary modulation orders of both the CCS and PSs. Numerical results show that, compared with conventional RSMA-based WBANs, SDSMA achieves significant SNR gains and latency reductions of more than 80% under the considered analytical processing-cycle model in both SISO and MIMO downlink settings.**

***Index Terms*—Wireless body area networks, low latency, parallel detection, interference management.**

I. Introduction

The rapid growth of the global aging population, together with sedentary lifestyles and poor dietary habits, is driving an unprecedented increase in chronic diseases [1]. As a result, real-time and continuous health monitoring has become increasingly important for early disease detection and reduced treatment costs [2]. Wireless body area networks (WBANs) have emerged as a promising solution, in which wearable sensors collect physiological information and transmit it to a body control unit (BCU), which then sends control signals to on-body actuators to respond promptly to abnormal patient conditions [3]. However, ensuring such prompt response remains challenging because of posture-induced fading, body shadowing, and strong intra- and inter-WBAN interference [4]. To mitigate interference, conventional WBANs typically employ multiple access (MA) schemes such as orthogonal multiple access (OMA) [5]; however, OMA does not fully exploit the limited spectrum [6]. Power-domain non-orthogonal MA (NOMA) improves spectral utilization [7], but it relies on multiple successive interference cancellation (SIC) stages, which incur high processing overhead that is undesirable for lightweight WBAN actuators. To overcome these drawbacks, single-layer multiple-input multiple-output (MIMO) rate-splitting MA (RSMA) has emerged as a flexible alternative [8], wherein each user message is divided into a common part (CP) and a private part (PP). The CPs of all users are jointly encoded into a single composite common stream (CCS), while each PP is encoded into a private stream (PS). At the receiver node, the CCS is first decoded in the presence of residual PS interference, after which each user retrieves its intended PS using a single SIC step. By partially decoding interference while treating the remaining interference as noise, RSMA mitigates interference more effectively than NOMA while reducing the number of SIC stages [8].

The flexibility of MIMO-RSMA and its applications are discussed in [9]. In healthcare, RSMA has been explored in fog-assisted architectures for joint uplink-downlink optimization [10] and in downlink WBAN scenarios [11]. Variants such as quadrature-splitting RSMA enhance reliability in low-power regimes [12], [13] and under imperfect SIC conditions [14]. Error-performance evaluations have also been reported in [15]–[19].

Despite the extensive literature on RSMA and its advantages, its application to WBANs remains limited, and conventional MIMO-RSMA is still not well matched to WBAN actuators. In conventional MIMO-RSMA, CCS decoding is impaired by residual PS interference, and each actuator must perform SIC before decoding its intended PS. This introduces receiver complexity and additional latency, which can scale with the number of actuators and is undesirable for ultra-low-power WBAN actuators operating under strict control-response deadlines. These limitations motivate a signaling strategy that enables interference-free CCS detection and parallel CCS/PS decoding with a single linear front-end. To the best of our knowledge, no existing MIMO-RSMA scheme for WBANs simultaneously achieves interference-free CCS detection, SIC-free PS decoding, and parallel CCS/PS decoding, although these features are critical for reliable, low-overhead control signaling in WBANs. Motivated by these limitations, we propose a *signal-space decoupled stream-splitting multiple access (SDSMA)* scheme for downlink MIMO-WBANs, in which the BCU maps the PSs onto the in-phase dimension of the baseband waveform, while the CCS is mapped onto the quadrature dimension. Although SDSMA follows the same message-splitting principle as RSMA, it departs from non-orthogonal signal superposition by separating the CCS and PSs across orthogonal signal-space dimensions. This design eliminates CCS contamination by PS interference, removes receiver-side SIC, and enables parallel CCS/PS decoding, which is particularly attractive for WBAN actuators with strict latency, energy, and control-response constraints. The key contributions of this work are summarized as follows:

1) We propose a lightweight MA scheme for downlink

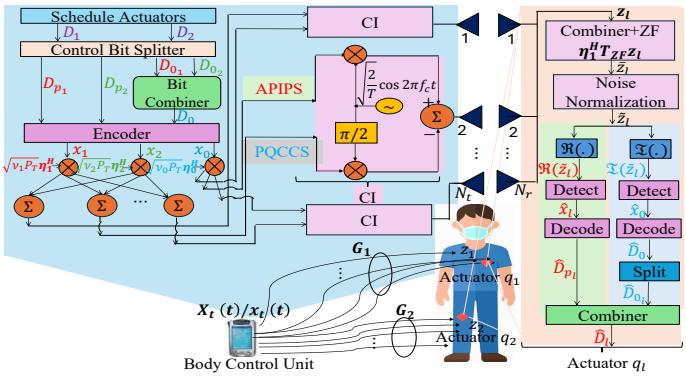

Figure 1. SDSMA based downlink MIMO-WBAN model.

MIMO-WBANs, termed SDSMA, that leverages orthogonal signal-space mapping of the CCS and PSs to enable SIC-free decoding.

2) We conduct a constellation-based error analysis to derive the exact symbol error rate (SER) of the proposed SDSMA for arbitrary modulation orders of both the CCS and PSs, along with closed-form average SER (ASER) expressions validated through extensive Monte Carlo simulations. We also extend the threshold-based detector (TBD) in [16] to the SDSMA in-phase superposition model to improve the detection reliability of power-imbalanced PSs, for which minimum-distance detectors (MDDs) become unreliable.
3) We demonstrate through analysis and simulation that SDSMA achieves significant SNR gains and more than 80% latency reduction compared with conventional RSMA-based WBAN downlinks under the same analytical processing-cycle model.

Remark 1. *While SDSMA is applicable to general MU-MIMO downlink channels, it is specifically motivated by WBAN actuators, where control reliability and decoding latency are safety-critical and SIC-induced sequential decoding is costly.*

II. WBAN System Model

Consider an SDSMA-based downlink MIMO-WBAN, where the BCU, equipped with N_t antennas, simultaneously delivers control signals to two on-body actuator nodes, denoted as q_1 and q_2, each equipped with N_r antennas, as illustrated in Fig. 1. The BCU acts as the on-body WBAN hub/controller and broadcasts safety-critical control information to actuators over short-range body-centric channels. For actuator (q_l), $l \in \mathcal{W} = \{1, 2\}$, a total of D_l control bits are transmitted per interval. These bits are logically partitioned into CP control bits (D_{0_l}) and PP control bits (D_{p_l}). The CP bits of both actuators are aggregated into a single composite control bitstream (D_0), which is encoded into the CCS (x_0). Each PP control bitstream (D_{p_l}) is independently encoded and mapped onto its respective PS (x_l). Each stream $x_k, \forall k \in \{0, 1, 2\}$ is drawn from a normalized ξ_k-ary constellation set, expressed as: $x_k \in \mathcal{X}_k = \left\{ \frac{(a_k - \xi_k)}{\sqrt{f_k}}; \forall a_k = 1, 3, \ldots, (2\xi_k - 1) \right\}$, where $f_k = \frac{(\xi_k{}^2 - 1)}{3}$ ensures $\mathbb{E}[|x_k|^2] = 1$. After precoding, the aggregate precoded in-phase PS (APIPS) and precoded quadrature CCS (PQCCS) baseband signals transmitted from all antennas are given by $\mathbf{x}_T^{Ip}(t) = \sum_{i=1}^{2} \sqrt{\nu_i P_T}\mathbf{x}_i(t)$ and $\mathbf{x}_T^{Qc}(t) = \sqrt{\nu_0 P_T}\mathbf{x}_0(t)$, respectively, where $\nu_k = \frac{\delta^k}{1+\delta+\delta^2}$ denotes the power allocation factor (PAF) satisfying $\sum_{k=0}^{2} \nu_k = 1$, δ $(0 < \delta < 1)$ is the weighting factor (WF), P_T is the total transmit power, and $\mathbf{x}_k(t) = \sum_m \mathbf{x}_k[m]g(t - mT_s)$ represents the precoded stream shaped by Nyquist pulse $g(t)$ with symbol duration $T_s = T$ and precoded symbol vectors $\mathbf{x}_k[m]$. The APIPS and PQCCS are modulated onto the carrier by multiplying $\mathbf{x}_T^{Ip}(t)$ with $\sqrt{\frac{2}{T}}\cos(2\pi f_c t)$ and $\mathbf{x}_T^{Qc}(t)$ with $\sqrt{\frac{2}{T}}\sin(2\pi f_c t)$ $\left(\cos\left(2\pi f_c t - \frac{\pi}{2}\right) = \sin(2\pi f_c t)\right)$, respectively. Subtracting the quadrature branch yields the overall bandpass transmitted signal:

$$\begin{aligned}\mathbf{X}_T(t) &= \mathbf{x}_{Ip}(t)\sqrt{\tfrac{2}{T}}\cos(2\pi f_c t) - \mathbf{x}_{Qc}(t)\sqrt{\tfrac{2}{T}}\sin(2\pi f_c t) \\ &= \sqrt{\tfrac{2}{T}}\Re\Big\{ \underbrace{\left(\mathbf{x}_{Ip}(t) + j\,\mathbf{x}_{Qc}(t)\right)}_{\mathrm{x}_T(t)\equiv \mathrm{x}_T} e^{\,j\,2\pi f_c t} \Big\}. \end{aligned} \tag{1}$$

Thus, the overall bandpass signal in (1) corresponds to the following equivalent complex baseband representation:

$$\mathbf{x}_T = \underbrace{\left(\sqrt{\nu_1 P_T}\mathbf{x}_1 + \sqrt{\nu_2 P_T}\mathbf{x}_2\right)}_{\text{APIPS}} + j\,\underbrace{\sqrt{\nu_0 P_T}\mathbf{x}_0}_{\text{PQCCS}}, \tag{2}$$

where $\mathbf{x}_T \in \mathbb{C}^{N_t \times 1}$ is the transmit vector across N_t antennas, $\mathbf{x}_k = \boldsymbol{\eta}_k^H x_k$ denotes the precoded stream with $\mathbb{E}[||\mathbf{x}_k||^2] = 1$, x_k is the encoded streams, $\boldsymbol{\eta}_k \in \mathbb{C}^{1 \times N_t}$ is the precoding vector satisfying $||\boldsymbol{\eta}_k||^2 = 1$, and $\mathbb{E}[\|\mathbf{x}_T\|^2] = P_T \sum_{k=0}^{2} \nu_k = P_T$.

Remark 2. *Geometrically, conventional RSMA produces constellations in which the CCS decision boundaries are shifted by the random realization of the PS symbols. In contrast, SDSMA makes the CCS decision boundaries invariant to the PS symbols because the CCS resides exclusively on the quadrature axis. This invariance increases the CCS minimum distance and improves reliability.*

Remark 3. *Although the analysis considers $\mathcal{W} = 2$ actuators for clarity, SDSMA can be extended to $\mathcal{W} > 2$ by mapping a CCS onto the quadrature dimension and superposing $\mathcal{W}$ PSs on the in-phase dimension. The CCS remains SIC-free and can still be decoded in parallel with the PS branch. However, generalized TBD is required to decode multiple lower-power PSs, as the number of decision regions increases with the number of superposed PS constellations. Thus, for large $\mathcal{W}$, SDSMA preserves parallel CCS/PS decoding while preventing complexity growth in the CCS branch.*

To facilitate a compact representation of the SER and ASER formulations, the unified symbol metric (Δ_{uq}^E) is defined as

$$\Delta_{uq}^E = \left(2E - d_u^{(q)} - \xi_{c^{(u)}}\right)\sqrt{\frac{\nu_{c^{(u)}}}{f_{c^{(u)}}}}, \tag{3}$$

where E is a scaling constant, $d_u^{(q)}$ corresponds to the q^{th} entry of the vector $[\mathbf{d}_u]_{1\times 6} = [1, 0, -\xi_{c^{(u)}}, -\xi_{c^{(u)}} - 1, \xi_{c^{(u)}} - 1, \xi_{c^{(u)}}]$, $c^{(u)}$ represents the u^{th} entry of the vector $\mathbf{c}_{1\times 3} = [1, 2, 0]$, $\nu_{c^{(u)}}$ is the PAF for the selected constellation point, and $f_{c^{(u)}}$ is the normalization factor ensuring unit average transmit power. The received signal vector at actuator q_l is

$$\mathbf{z}_l = \mathbf{G}_l\mathbf{x}_T + \boldsymbol{\omega}_l, \tag{4}$$

where $\mathbf{G}_l \in \mathbb{C}^{N_r \times N_t}$ is the channel matrix between the BCU and q_l, $\boldsymbol{\omega}_l \in \mathcal{CN}(\mathbf{0}, \Omega_l^2\mathbf{I}_{N_r})$ denotes the additive white Gaussian noise (AWGN) vector, $\mathbf{0}$ is the $N_r \times 1$ zero vector, Ω_l^2 is the

noise variance, and $\mathbf{I}_{N_r}$ is the identity matrix. To facilitate decoding, actuator q_l applies a zero-forcing (ZF) equalizer $\mathbf{T}_{ZF} = \left(\mathbf{G}_l^H \mathbf{G}_l\right)^{-1} \mathbf{G}_l^H$, to $\mathbf{z}_l$. This is followed by a linear combiner $\boldsymbol{\eta}_l^H$, yielding the effective received signal for $N_r \geq N_t$ as $\bar{z}_l = \boldsymbol{\eta}_l \mathbf{T}_{ZF} \mathbf{z}_l = x_T + \bar{\omega}_l$, where $x_T = \sqrt{\nu_1 P_T} x_1 + \sqrt{\nu_2 P_T} x_2 + j\sqrt{\nu_0 P_T} x_0$, and $\bar{\omega}_l \sim \mathcal{CN}\left(0, \Omega_l^2 \boldsymbol{\eta}_l \left(\mathbf{G}_l^H \mathbf{G}_l\right)^{-1} \boldsymbol{\eta}_l^H\right)$ denotes the equivalent AWGN. To isolate the gain due to signal-space decoupling rather than precoder optimization, fixed unit-norm equal-gain precoders are used and are set as $\boldsymbol{\eta}_l = \boldsymbol{\eta}_k = \frac{1}{\sqrt{N_t}} \mathbf{1}_{1\times N_t}, \forall\, l, k$, $\mathbf{1}$ is an all-ones row vector. Normalizing the noise to unit variance yields $\tilde{z}_l = \frac{\bar{z}_l}{\sqrt{\Omega_l^2 \boldsymbol{\eta}_l (\mathbf{G}_l^H \mathbf{G}_l)^{-1} \boldsymbol{\eta}_l^H}} = \sqrt{\rho M_l} \tilde{x}_T + \tilde{\omega}_l$, where $\rho = \frac{P_T}{\Omega_l^2}$ is the average signal-to-noise ratio (SNR), $\tilde{x}_T = \sqrt{\nu_1} x_1 + \sqrt{\nu_2} x_2 + j\sqrt{\nu_0} x_0$, $M_l = \frac{1}{\boldsymbol{\eta}_l (\mathbf{G}_l^H \mathbf{G}_l)^{-1} \boldsymbol{\eta}_l^H}$, and $\tilde{\omega}_l \sim \mathcal{CN}(0,1)$. Each actuator q_l extracts the quadrature component ($\Im\{\tilde{z}_l\}$) to detect (x_0) using the MDD rule:

$$\hat{x}_0 = \arg \min_{x_0 \in \mathcal{X}_0} \left| \Im\{\tilde{z}_l\} - \sqrt{\rho M_l \nu_0} x_0 \right|, \tag{5}$$

where $\hat{x}_0 \in \mathcal{X}_0$ is the detected control CCS.

Remark 4. *In WBANs, the CCS conveys safety-critical control bits that must be decoded reliably at all actuators under strict response-time constraints, which motivates interference-free CCS detection without SIC.*

Concurrently, each actuator q_l detects its intended control PS (x_l) from the in-phase component $\Re\{\tilde{z}_l\}$. If the PS of q_l is allocated the highest transmit power, detection is performed using MDD as

$$\hat{x}_1 = \arg \min_{x_1 \in \mathcal{X}_1} \left| \Re\{\tilde{z}_l\} - \sqrt{\rho M_l \nu_1} x_1 \right|, \tag{6}$$

where $\hat{x}_1 \in \mathcal{X}_1$ is the detected control PS for actuator q_1. Since $\Im\{\tilde{z}_l\}$ contains only the CCS, no additional power-allocation constraints are required for reliable MDD of x_0 (Eq. 5). However, reliable MDD of x_1 (Eq. (6)) requires avoiding decision-region overlap by satisfying the inequality: $-\Delta_{11}^{\xi_1} + \Delta_{21}^{\xi_2} \leq -\Delta_{11}^{\xi_1 - 1} - \Delta_{21}^{\xi_2}$. From this, the following PAF and WF constraints are obtained: $\mathbf{C1}: \sqrt{\frac{\nu_1}{(\xi_1^2-1)}} > (\xi_2 - 1)\sqrt{\frac{\nu_2}{(\xi_2^2-1)}}$, which, in terms of the WF parameter, yields $\delta < \delta_M$, where $\delta_M = \frac{(\xi_2+1)}{(\xi_2-1)(\xi_1^2-1)}$. When the PS of q_k is allocated lower power than a competing PS, conventional MDD becomes unreliable because the decision boundaries are derived assuming a single active PS and therefore ignore the displacement caused by higher-power PS interference. As a result, the effective constellation of the lower-power PS is distorted, leading to significant detection errors. To address this issue, detection of x_2 is performed using the TBD approach [16], which accounts for the power asymmetry and mitigates decision-region overlap:

$$\hat{x}_2 \in \begin{cases} \hat{x}_2^{(1)}, \text{ if } (\Upsilon_l \leq \mathrm{DB}_1) \bigcup_{\varpi_1=2}^{\xi_1} (\mathrm{DB}_2^{\varpi_1} \leq \Upsilon_l \leq \mathrm{DB}_3^{\varpi_1}) \\ \hat{x}_2^{(\varrho)}, \text{ if } \bigcup_{\varpi_1=1}^{\xi_1} \mathrm{DB}_4^{\varpi_1 \varrho} \leq \Upsilon_l \leq \mathrm{DB}_5^{\varpi_1 \varrho}, \\ \hat{x}_2^{(\xi_2)}, \text{if } (\Upsilon_l \geq \mathrm{DB}_6) \bigcup_{\varpi_1=1}^{\xi_1 - 1} (\mathrm{DB}_7^{\varpi_1} \leq \Upsilon_l \leq \mathrm{DB}_8^{\varpi_1}) \end{cases} \tag{7}$$

where $\hat{x}_2^{(.)}$ denotes the $(.)^{th}$ entry of the detected symbol vector $\hat{x}_2$, $\varrho \in \{2, 3, \cdots (\xi_2 - 1)\}$, $\Upsilon_l = \frac{\Re\{\tilde{z}_l\}}{\sqrt{\rho M_l}}$, $\mathrm{DB}_1 = \Delta_{11}^1 + \Delta_{22}^1$, $\mathrm{DB}_2^{\varpi_1} = \Delta_{12}^{\varpi_1 - 1}$, $\mathrm{DB}_3^{\varpi_1} = \Delta_{11}^{\varpi_1} + \Delta_{22}^1$, $\mathrm{DB}_4^{\varpi_1 \varrho} = \Delta_{11}^{\varpi_1} + \Delta_{22}^{\varrho - 1}$, $\mathrm{DB}_5^{\varpi_1 \varrho} = \Delta_{11}^{\varpi_1} + \Delta_{22}^{\varrho}$, $\mathrm{DB}_6 = \Delta_{11}^{\xi_1} + \Delta_{22}^{\xi_2 - 1}$, $\mathrm{DB}_7^{\varpi_1} = \Delta_{11}^{\varpi_1} + \Delta_{22}^{\xi_2 - 1}$, and $\mathrm{DB}_8^{\varpi_1} = \Delta_{12}^{\varpi_1}$.

Remark 5. *The TBD is a structured decision-region detector introduced in [16] for RSMA constellations and extended here to the SDSMA in-phase superposition model, where the decision thresholds are derived analytically from the in-phase superposed constellation geometry of the PSs. It overcomes the limitations of MDDs in the presence of mixed power streams.*

III. Constellation-Based Error Analysis

A. SER for the PS and CCS of q_l

The SER of the control PS symbol (x_l) is defined as $\mathrm{Pe}_{x_l} = 1 - \mathrm{Pc}_{x_l}$, where Pc_{ς} denotes the correct symbol rate (CSR) of control stream ς. For the PS of actuator q_l, it is given by

$$\begin{aligned} \mathrm{Pc}_{x_l} &= \sum_{\varpi_1 = \varpi_2 = 1}^{\xi_l} \Pr(x_l^{(\varpi_1)}, \hat{x}_l^{(\varpi_2)}) \\ &= 2 \sum_{\substack{\tau_t = 1 \\ t \neq l}}^{\xi_t} \Pr\left(x_l^{(1)}, \hat{x}_l^{(1)}, x_t^{(\tau_t)}\right) + (\xi_l - 2) \sum_{\substack{\tau_t = 1 \\ t \neq l}}^{\xi_t} \Pr\left(x_l^{(2)}, \hat{x}_l^{(2)}, x_t^{(\tau_t)}\right), \end{aligned} \tag{8}$$

where $x_l^{(\varpi_1)}$ and $\hat{x}_l^{(\varpi_2)}$ denote the ϖ_1^{th} and ϖ_2^{th} entries of the constellation $\mathcal{X}_l$, respectively. Exploiting constellation symmetry yields the first equality: $\Pr(x_l^{(1)}, \hat{x}_l^{(1)}) = \Pr(x_l^{(\xi_l)}, \hat{x}_l^{(\xi_l)})$, and the second equality follows from $\Pr(x_l^{(p)}, \hat{x}_l^{(p)}) = \Pr(x_l^{(2)}, \hat{x}_l^{(2)}), \forall p \in \{3, 4, \cdots, \xi_l - 1\}$. These joint probabilities capture the likelihood of correctly detecting the target control PS symbols $x_l^{(1)}$ or $x_l^{(2)}$ given all possible realizations of the interfering control PS symbols $x_t, \forall t \neq l$, which are assumed to be uniformly distributed, i.e., $\Pr(x_t) = \frac{1}{\xi_t}$. Since $\Pr(x_l) = \frac{1}{\xi_l}$, Eq.(8) can be reformulated as

$$\begin{aligned} \mathrm{Pc}_{x_l} = \frac{2}{\xi_1 \xi_2} \sum_{\substack{\tau_t = 1 \\ t \neq l}}^{\xi_t} \underbrace{\Pr\left(\hat{x}_l^{(1)} \parallel x_l^{(1)}, x_t^{(\tau_t)}\right)}_{\Omega_1} \\ + \frac{(\xi_l - 2)}{\xi_1 \xi_2} \sum_{\substack{\tau_t = 1 \\ t \neq l}}^{\xi_t} \underbrace{\Pr\left(\hat{x}_l^{(2)} \parallel x_l^{(2)}, x_t^{(\tau_t)}, \right)}_{\Omega_2}, \end{aligned} \tag{9}$$

where the terms Ω_1 and Ω_2 in (9) are obtained via constellation-based detection analysis and are expressed as follows:

$$\begin{aligned} \Omega_1 &= Q\left(-\sqrt{2\rho M_l} \zeta_1^{\tau_t}\right) + Q\left(\sqrt{2\rho M_l} \zeta_2^{\tau_t}\right) - Q\left(\sqrt{2\rho M_l} \zeta_3^{\tau_t}\right) \\ &+ (l-1) \sum_{u_1=1}^{2} \sum_{\substack{u_t = 2 \\ t \neq l}}^{\xi_t - 1} Q\left(\sqrt{2\rho M_l} \zeta_4^{\tau_t \mathbf{u}}\right) - Q\left(\sqrt{2\rho M_l} \zeta_5^{\tau_t \mathbf{u}}\right), \end{aligned} \tag{10}$$

and

$$\Omega_2 = \sum_{u_1=1}^{2} \sum_{\substack{u_t = 1 \\ l \neq 1, t \neq l}}^{\xi_t} \left(Q\left(\sqrt{2\rho M_l} \zeta_6^{\tau_t \mathbf{u}}\right) - Q\left(\sqrt{2\rho M_l} \zeta_7^{\tau_t \mathbf{u}}\right)\right), \tag{11}$$

where $Q(\cdot)$ denotes the Gaussian Q-function, $\mathbf{u} = [u_1, u_2]$, $\zeta_1^{\tau_t} = \Delta_{l4}^0 + (l-1)\Delta_{\tilde{l}1}^1 - \Delta_{\tilde{l}1}^{\tau_t}$, $\zeta_2^{\tau_t} = -\Delta_{l1}^1 - \Delta_{\tilde{l}1}^{\tau_t}$, $\zeta_3^{\tau_t} = \Delta_{l4}^0 + (l-1)\Delta_{\tilde{l}1}^1 - \Delta_{\tilde{l}1}^{\tau_t}$, $\zeta_4^{\tau_t \mathbf{u}} = \Delta_{\tilde{l}4}^{u_t - \tau_t - 1} - \Delta_{l1}^1$, $\zeta_5^{\tau_t \mathbf{u}} = \Delta_{\tilde{l}3}^{u_t - \tau_t} + \Delta_{l4}^0$, $\zeta_6^{\tau_t \mathbf{u}} = -\Delta_{l4}^0 + (l-1)\Delta_{\tilde{l}1}^{u_t} - \Delta_{\tilde{l}1}^{\tau_t}$, and $\zeta_7^{\tau_t \mathbf{u}} = \Delta_{l4}^0 + (l-1)\Delta_{\tilde{l}1}^{u_t} - \Delta_{\tilde{l}1}^{\tau_t}$, with $\tilde{l} = 3 - l$. Substituting (10) and (11) into (9), and subsequently into Pe_{x_l} expression, yields the SER for x_l. Similarly, the SER for the CCS (x_0) is $\mathrm{Pe}_{x_0} = 1 - \mathrm{Pc}_{x_0}$, where Pc_{x_0} is expressed as

$$\mathrm{Pc}_{x_0} = \frac{2}{\xi_0} \underbrace{\Pr\left(\hat{x}_0^{(1)} \parallel x_0^{(1)}\right)}_{\Omega_3} + \frac{(\xi_0 - 2)}{\xi_0} \underbrace{\Pr\left(\hat{x}_0^{(2)} \parallel x_0^{(2)}\right)}_{\Omega_4}. \tag{12}$$

The terms Ω_3 and Ω_4 follow the same procedure as in (9)-(11) and are therefore given by

$$\mathrm{Pc}_{x_0} = 1 - \frac{2(\xi_0 - 1)}{\xi_0} Q\left(\sqrt{2\rho M_l} \zeta_{34}^0\right). \tag{13}$$

Finally, substituting (13) into Pe_{x_0} yields the SER of x_0.

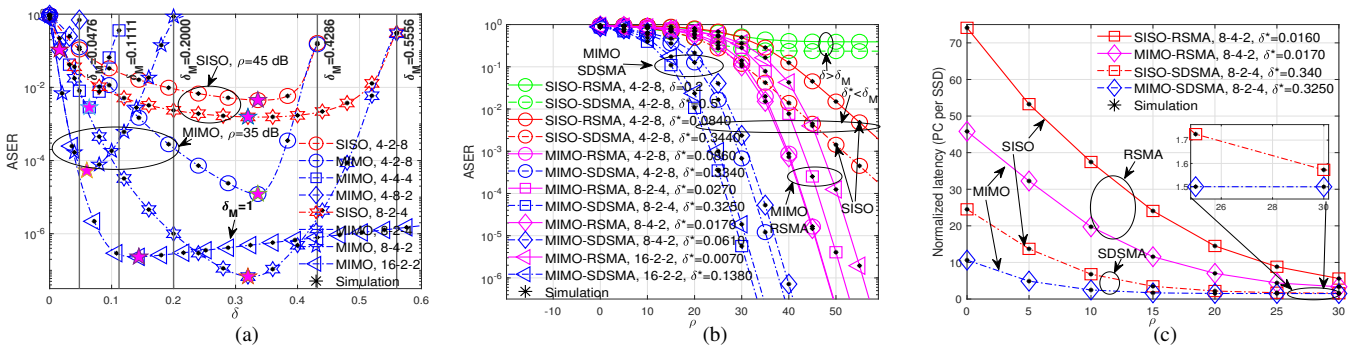

Figure 2. (a) ASER of SDSMA versus WF for SISO ($N_t=1, N_r=1$) and MIMO ($N_t=3, N_r=6$); (b) ASER comparison of RSMA and SDSMA under SISO and MIMO; and (c) Normalized latency in PC per SSD for RSMA and SDSMA.

B. Overall SER and ASER Expressions

To ensure reliable detection of the control CCS at both actuators, the minimum CSR across actuators is considered. Accordingly, the instantaneous overall SER of the MIMO-WBAN system is expressed as $\mathrm{Pe}^{\mathrm{ovl}} = 1 - \mathrm{Pc}_{x_0}^{\min}\mathrm{Pc}_{x_1}\mathrm{Pc}_{x_2}$, where $\mathrm{Pc}_{x_0}^{\min} = \min_{l\in\mathcal{W}}\mathrm{Pc}_{x_0} = \mathrm{Pc}_{x_0}|_{M_l=\min(M_1,M_2)}$ denotes the minimum CSR of x_0 across both actuators. To compute the ASER for actuator q_l, each Gaussian term of the form $Q(\vartheta\sqrt{M_l})$, where $\vartheta > 0$ is a constant, appearing in the expressions for Pe_{x_l} and Pe_{x_0}, must be averaged over the PDF of M_l. Following [20], $M_l = \frac{1}{\boldsymbol{\eta}_l(\mathbf{G}_l^H\mathbf{G}_l)^{-1}\boldsymbol{\eta}_l^H}$ is Gamma distributed with shape parameter $\lambda = N_r - N_t + 1$, and scale parameter $\kappa = 1$, whose probability density function (PDF) is given by $f_{M_l} = \frac{1}{\Gamma(\lambda)\kappa^\lambda}M_l^{\lambda-1}e^{-M_l/\kappa}, \quad M_l > 0$. Therefore, its averaging integral is

$$\mathcal{T}_l(\vartheta) = \int_0^\infty Q\left(\vartheta\sqrt{M_l}\right)\frac{1}{\Gamma(\lambda)\,\kappa^\lambda}\,M_l^{\lambda-1}e^{-M_l/\kappa}dM_l. \tag{14}$$

The integral in (14) can be evaluated using MATHEMATICA© as follows:

$$\mathcal{T}_l(\vartheta) = \frac{4^{-\lambda}\kappa^{-\lambda}\vartheta^{-2\lambda}\Gamma(2\lambda)}{\Gamma(\lambda)}G_{2,2}^{1,2}\left(-\frac{1}{\kappa\vartheta^2}\middle|\begin{matrix}1-\lambda, \frac{1}{2}-\lambda\\ 0, -\lambda\end{matrix}\right), \tag{15}$$

where $G_{\cdot,\cdot}^{\cdot,\cdot}(.|^{\cdots}_{\cdots})$ is Meijer G-function. By substituting $\mathcal{T}_l(\vartheta)$ from (15)) for each Gaussian $Q(\cdot)$ term in the expression for Pe_{x_l} after substituting Pc_{x_l} from Eqs. (9)-(11), and in the expression for Pe_{x_0} after substituting Pc_{x_0} from Eq. (13), the analytical ASER expressions for the control PS and CCS are obtained. Therefore, the overall system ASER is computed as:

$$\bar{\mathrm{Pe}}^{\mathrm{ovl}} = 1 - \bar{\mathrm{Pc}}_{x_0}^{\min}\bar{\mathrm{Pc}}_{x_1}\bar{\mathrm{Pc}}_{x_2}, \tag{16}$$

where $\bar{\mathrm{Pc}}_{x_0}^{\min} = \mathbb{E}[\mathrm{Pc}_{x_0}^{\min}]$ and $\bar{\mathrm{Pc}}_{x_l} = \mathbb{E}[\mathrm{Pc}_{x_l}]$ denote the average CSR (ACSR) for x_0 and x_l, respectively.

IV. Numerical Results and Discussion

This section validates the derived analytical ASER expressions of the proposed SDSMA scheme under both SISO ($N_t = 1, N_r = 1$) and MIMO ($N_t = 3, N_r = 6$) configurations through Monte Carlo simulations over 10^8 independent channel realizations. In all figures, the legend notation $\xi_0 - \xi_1 - \xi_2$ indicates that stream x_k employs a ξ_k-ary constellation. For performance comparison, single-layer RSMA is adopted as the baseline scheme because it is a widely used message-splitting framework for MU-MIMO systems and subsumes NOMA [8]. Therefore, performance gains over RSMA also indicate improvements over conventional MA schemes.

Figure 2(a) illustrates the ASER variation with respect to the WF (δ), evaluated at $\rho = 45$ dB for SISO and $\rho = 35$ dB for MIMO. The plot extends up to δ_{M} (threshold values shown in Fig. 2(a)) for all combinations of modulation orders $\xi_0 - \xi_1 - \xi_2$ corresponding to a total of 6 information bits, with 3 information bits per actuator (IBPA). The curves exhibit a convex trend, confirming the existence of an optimal WF $\delta^\star$ that minimizes $\bar{P}_{\mathrm{e}}^{\mathrm{ovl}}$. The optimal points, marked with magenta stars ($\star$), consistently satisfy constraint **C1**, that is, $\delta^\star < \delta_{\mathrm{M}}$. For MIMO, $\delta^\star$ takes the values 0.3340, 0.0650, 0.0170, 0.3250, 0.0610, 0.1380 for 4-2-8, 4-4-4, 4-8-2, 8-2-4, 8-4-2, 16-2-2, respectively, while for SISO, $\delta^\star$ takes the values 0.3440 and 0.340 for 4-2-8 and 8-2-4, respectively. These results show that the transition from SISO to MIMO induces only marginal shifts in $\delta^\star$, indicating robustness with respect to antenna dimensions. Among all tested configurations, 8-2-4 achieves the lowest ASER. This behavior arises because, when an odd π IBPA is available, assigning one bit to the PS of q_1, $\pi - 1$ bits to the PS of q_2 (which has lower power allocation, i.e., $\nu_2 < \nu_1$), and π bits to the CCS yields a more balanced error performance.

Figure 2(b) presents the ASER versus SNR for SISO and MIMO configurations, with each curve evaluated at its corresponding optimal WF $\delta^\star$. The analytical results closely match the Monte Carlo simulations, validating the derived closed-form expressions. As expected, all curves exhibit waterfall behavior with increasing SNR, while SDSMA consistently outperforms RSMA across modulation orders and antenna configurations. This gain is directly tied to the SDSMA signal design: the CCS is decoded from the interference-free quadrature component, unlike in RSMA, where CCS decoding suffers from residual PS interference. As a result, for the same power split ν_k, SDSMA provides a larger effective minimum distance for CCS decisions. In addition, SDSMA offers *interference-free CCS detection*, *eliminates SIC error propagation*, and *supports parallel CCS/PS decoding*, which jointly improve reliability and reduce latency. The figure also confirms that the 8-2-4 allocation yields the lowest ASER across the considered SNR range. In the SISO case with a 4-2-8 allocation, SDSMA achieves an ASER of 10^{-3} with nearly 10 dB less SNR than SISO-RSMA. Similarly, for MIMO with an 8-4-2 allocation, SDSMA requires about 20 dB less SNR than MIMO-RSMA to attain an ASER of 10^{-5}, demonstrating

substantial SNR efficiency. Moreover, the MIMO-SDSMA curves exhibit a steeper slope in the high-SNR regime than their SISO counterparts, reflecting the diversity gain provided by multiple antennas. For example, MIMO-SDSMA reduces ASER from 10^{-2} at $\rho = 20$ dB to 10^{-5} at $\rho = 30$ dB, resulting in diversity $\approx -\frac{\log_{10}(10^{-5})-\log_{10}(10^{-2})}{(30-20)/10} = 3$, while SISO-RSMA achieves only diversity $= 1$. To evaluate the role of the WF constraint **C1**, Fig. 2(b) also depicts the ASER when ($\delta < \delta_{\mathrm{M}}$) is intentionally violated. Once ($\delta > \delta_{\mathrm{M}}$), the ASER curves deviate sharply, leading to substantially higher error rates compared to those in the feasible region. This degradation confirms the necessity of **C1**, as ignoring it results in severe decision-region overlap and significant performance loss.

Figure 2(c) evaluates the normalized latency (NL), expressed in processing cycles per successful symbol detection (PC per SSD), to reflect the actuator-side computation limits typical of WBAN nodes: $\mathcal{L} = \frac{\mathcal{T}^{\mathrm{SDSMA}}}{\max(\bar{\mathrm{P}}\mathrm{c}^{\mathrm{ovl}},\varepsilon)}$, where $\mathcal{T}^{\mathrm{SDSMA}} = T_p + \max(T_{x_0}, T_{x_l})$ is the total processing delay, T_p is the preprocessing cost (e.g., combiner and ZF equalization), T_{x_k} is the detection time of stream x_k, $\bar{\mathrm{P}}\mathrm{c}^{\mathrm{ovl}} = 1 - \bar{\mathrm{P}}\mathrm{e}^{\mathrm{ovl}}$ denotes the ACSR, and $\varepsilon \approx 2.2204 \times 10^{-16}$ prevents division by zero. Since SDSMA supports parallel decoding of x_0 and x_l, the maximum of the two detection times is considered. In contrast, RSMA latency includes sequential decoding overhead, such that $\mathcal{T}^{\mathrm{RSMA}} = T_p + T_{\mathrm{SIC}} + T_{x_0} + T_{x_l}$, where T_{SIC} is the additional SIC delay in RSMA. Considering $T_p = 0.5$, $T_{\mathrm{SIC}} = 0.5$, and $T_{x_k} = 1$, Fig. 2(c) compares the NL performance of SDSMA at its best $8-2-4$ configuration (as per Figs. 2(a) and 2(b)) and RSMA at its best $8-4-2$ configuration (as per Fig. 2(a)) for both SISO and MIMO settings. The figure confirms that simulation markers align with analytical curves, thereby validating the latency model. Across all scenarios, latency decreases with increasing ρ because improved symbol reliability reduces the need for retransmissions. More importantly, SDSMA consistently achieves lower NL than RSMA in both SISO and MIMO settings. For example, at $\rho = 10$ dB, MIMO-SDSMA yields $\mathcal{L} \approx 2.48$ versus 19.73 for MIMO-RSMA, corresponding to an 87.4% reduction. Similarly, SISO-SDSMA achieves $\mathcal{L} \approx 6.79$ compared to 37.44 for SISO-RSMA, corresponding to an 81.9% reduction. These improvements arise from interference-free CCS detection, simultaneous CCS-PS decoding, and elimination of SIC overhead. In addition, the improved CCS reliability in SDSMA lowers the retransmission probability, which further reduces the processing cycles per successful detection. In contrast, in RSMA, CCS errors can trigger SIC failure and repeated decoding, thereby increasing both processing cost and latency.

V. Conclusion

This paper proposed SDSMA for downlink MIMO-WBANs, where the CCS and PSs are separated across orthogonal signal-space dimensions to enable interference-free CCS detection and simultaneous SIC-free CCS/PS decoding, thereby reducing actuator complexity. A rigorous constellation-based error analysis was conducted, and exact SER as well as closed-form ASER expressions were derived for arbitrary modulation orders of both the CCS and PSs. Numerical results validated the analysis and showed that SDSMA achieves substantial SNR gains and reduces decoding latency by more than 80% compared to conventional RSMA-based WBAN downlinks under the considered analytical processing-cycle model. These results indicate that SDSMA is a promising low-complexity transmission framework for latency-critical and reliability-sensitive WBAN control applications. Future work may extend the framework to multi-hop cooperative WBANs with imperfect channel knowledge and hardware impairments.

References

[1] R. W. Kimokoti *et al.*, "Nutrition for the prevention of chronic diseases," *Medical Clinics*, vol. 100, no. 6, pp. 1185–1198, 2016.

[2] K. He *et al.*, "Early detection and risk assessment for chronic disease with irregular longitudinal data analysis," *J. Biomed. Inform.*, vol. 96, p. 103231, 2019.

[3] A. Salehi Shahraki *et al.*, "Access control, key management, and trust for emerging wireless body area networks," *Sensors*, vol. 23, no. 24, p. 9856, 2023.

[4] P. Majumdar *et al.*, "A survey on data-driven approaches for reliability, robustness, and energy efficiency in wireless body area networks," *Sensors (Basel, Switzerland)*, vol. 24, no. 20, p. 6531, 2024.

[5] S. Ullah *et al.*, "A study of MAC protocols for WBANs," *Sensors*, vol. 10, no. 1, pp. 128–145, 2009.

[6] P. Jain *et al.*, "Performance evaluation of cooperative OMA and NOMA systems in 6G deployment scenarios," *Sensors*, vol. 22, no. 11, p. 3986, 2022.

[7] A. S. Shah *et al.*, "Survey and performance evaluation of multiple access schemes for next-generation wireless communication systems," *IEEE Access*, vol. 9, pp. 113 428–113 442, 2021.

[8] Y. Mao *et al.*, "Rate-splitting multiple access for downlink communication systems: bridging, generalizing, and outperforming SDMA and NOMA," *EURASIP J Wirel Commun Netw*, vol. 2018, no. 1, pp. 1–54, 2018.

[9] ——, "Rate-splitting multiple access: Fundamentals, survey, and future research trends," *IEEE Commun. Surv. Tutor.*, vol. 24, no. 4, pp. 2073–2126, 2022.

[10] J. Zhou *et al.*, "Joint uplink and downlink rate splitting for fog computing-enabled internet of medical things," *IEEE Internet Things J.*, 2024.

[11] G. Arora *et al.*, "Downlink WBAN actuation via RSMA: Exact error analysis for nakagami-m fading," in *Proc. IEEE Int. Conf. Adv. Netw. Telecommun. Syst. (ANTS)*, 2025, pp. 1–6.

[12] ——, "Zero SIC based rate splitting multiple access technique," *IEEE Commun. Lett.*, vol. 26, no. 10, pp. 2430–2434, 2022.

[13] ——, "Sum-rate maximization under unequal rate allocation in downlink Q-RSMA," in *Proc. IEEE Int. Conf. Adv. Netw. Telecommun. Syst. (ANTS)*, 2024, pp. 1–6.

[14] ——, "A novel quadrature stream-splitting integrated SIC-driven multiple access scheme for enhanced performance under imperfect SIC," *IEEE Wirel. Commun. Lett.*, 2025.

[15] X. Su *et al.*, "Performance analysis of rate splitting in k-user interference channel under imperfect CSIT: Average sum rate, outage probability and SER," *IEEE Access*, vol. 8, pp. 136 930–136 946, 2020.

[16] G. Arora *et al.*, "Constellation based symbol error rate and power constraint analysis for RSMA," in *Proc. IEEE Int. Conf. Commun. (ICC)*, 2023, pp. 6627–6633.

[17] ——, "Optimal modulation order and power allocation for rate-splitting multiple access scheme," in *IEEE Nat. Conf. Commun. (NCC)*, 2025, pp. 1–6.

[18] ——, "Multi-user rate-splitting approach for enhanced private stream interference management with error and power bound analysis," *IEEE Trans. Wireless Commun.*, vol. 25, pp. 11 143–11 160, 2026.

[19] ——, "Coded error performance analysis for RSMA over nakagami-m fading with transceiver hardware impairments," *IEEE Trans. Commun.*, vol. 74, pp. 4090–4107, 2026.

[20] D. Gore *et al.*, "Transmit selection in spatial multiplexing systems," *IEEE Commun. Lett.*, vol. 6, no. 11, pp. 491–493, 2002.